Analytical Derivation of Phase Current Waveform Eliminating Torque Ripple and Input Current Ripple of Switched Reluctance Motors under Magnetically Saturated Operation

Takayuki Kusumi, Kosuke Kobayashi, Kazuhiro Umetani, Eiji Hiraki
Graduate School of Natural Science and Technology
Okayama University
Okayama, Japan

Published in: 2019 IEEE Energy Conversion Congress and Exposition (ECCE)

DOI: 10.1109/ECCE.2019.8912726

Analytical Derivation of Phase Current Waveform Eliminating Torque Ripple and Input Current Ripple of Switched Reluctance Motors under Magnetically Saturated Operation

Takayuki Kusumi
Graduate School of Natural Science and Technology
Okayama University
Okayama, Japan
p75s6ovi@s.okayama-u.ac.jp

Kosuke Kobayashi
Graduate School of Natural Science and Technology
Okayama University
Okayama, Japan
pn9p7rfd@s.okayama-u.ac.jp

Kazuhiro Umetani
Graduate School of Natural Science and Technology
Okayama University
Okayama, Japan
umetani@okayama-u.ac.jp

Eiji Hiraki
Graduate School of Natural Science and Technology
Okayama University
Okayama, Japan
hiraki@okayama-u.ac.jp

***Abstract*— Switched reluctance motors (SRMs) is beneficial in excellent cost-effectiveness and high thermal tolerance owing to their simple mechanical construction free from permanent magnets. Nevertheless, application of SRMs to vehicular propulsion is often hindered by their comparatively large input current ripple and torque ripple. For mitigating the problem, the previous study has proposed a phase current waveform that eliminates both of these ripples under the magnetization below the magnetic saturation. However, this previous technique still suffers from significant torque and input current ripples at large output torque, which tends to cause the magnetic saturation. This paper proposes an improved phase current waveform that eliminates these ripples even at large output torque. This waveform was derived analytically based on the nonlinear magnetic model of the SRM. The proposed phase current waveform was successfully verified by the experiment, suggesting the usefulness of the proposed technique for applying SRMs to vehicular propulsion.**

Keywords—input current ripple, magnetic saturation, phase current waveform, switched reluctance motor, torque ripple

I. INTRODUCTION

The switched reluctance motor (SRMs) is a reluctance motor that does not contain permanent magnets. Owing to their simple mechanical construction, SRMs can exhibit excellent cost-effectiveness and high thermal tolerance with comparatively high power density. Therefore, SRMs are now emerging as a promising candidate as propulsion motors for electric vehicles (EVs) [1].

In spite of the attractive features, however, the practical application of SRMs is hindered by comparatively large input current ripple and torque ripple [1][2]. Large input current ripple may deteriorate the lifespan of the batteries. Particularly, low-frequency input current ripple generated by the cycle of the phase current is difficult to be decoupled by the input smoothing capacitor of the inverter. On the other hand, large torque ripple tends to deteriorate driving comfort by severe noise vibration. Particularly, low-frequency torque ripple is also difficult to be decoupled by the inertia of the motor. Therefore, practical vehicular propulsion requires the SRM drive that can eliminate both of the input current ripple and the torque ripple simultaneously.

Conventionally, a number of studies have been dedicated to reducing these ripples [3]–[32]. Particularly, reduction of the torque ripple was energetically studied in the preceding studies [3]–[30]. These studies can be mainly categorized into two approaches. One is the optimization of the physical motor structure. The other is the optimization of the phase current waveform. Meanwhile, reduction of the input current ripple has been targeted by fewer studies compared with the torque ripple. However, [31][32] reported a successful reduction of the input current ripple by proposing a special inverter topology driven by a novel control technique. These preceding techniques [3]–[32], addressing these two types of ripples, were proven to be effective. Nonetheless, the majority of them can only reduce either one of the torque ripple and the input current ripple. Therefore, the simultaneous elimination of these ripples is still a challenging issue.

Certainly, there are a few techniques that can reduce both of these ripples simultaneously [33]–[36]. The reason for comparatively large ripples of the SRMs is originated from the two features of the phase inductance profile, i.e. the dependence of the phase inductance on the electric angle: One is the high-order harmonics contained in the phase inductance profile; and the other is the nonlinear dependence of the phase inductance on the phase magnetic flux due to the magnetic saturation. These preceding techniques consider the former feature and proposed propulsion method to eliminate both of the input current ripple and the torque ripple.

Conventionally, [33][34] proposed utilization of a special SRM structure named the pseudo-sinusoidal SRM, which has the inductance profile close to the sinusoidal wave, to avoid the former feature. Therefore, this technique is difficult to be applied to the commercially available SRMs. In order to avoid this problem, [35][36] recently proposed a derivation method of the phase current waveform that can eliminate both of the input current ripple and the torque ripple without using the sinusoidal phase inductance profile. This method

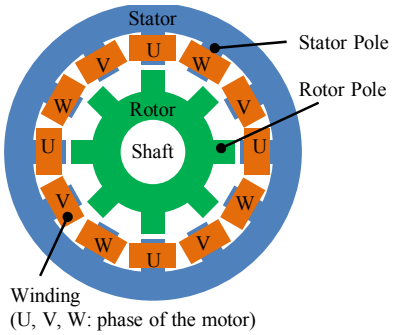

Fig. 1. Three-phase SRM under consideration

can be universally applied to the SRMs with arbitrary inductance profile, including the commercially available SRMs. The effective elimination of these ripples was experimentally proven at a low torque operation, in which the magnetic saturation scarcely occurs. Nevertheless, this technique neglects the latter feature of the phase inductance profile. Therefore, this technique still suffers from an insufficient reduction of these ripples at large output torque because the magnetic saturation cannot be neglected.

The purpose of this paper is to improve this previous technique to cover higher torque operation by further considering the latter feature. For this purpose, this paper derives the phase current waveform based on the nonlinear magnetic model of the SRMs, in which the magnetic co-energy contributed by a phase is given as a nonlinear function of the electric angle and the phase current.

This paper derives the phase current waveform using the analytical calculation rather than the numerical calculation. Certainly, the recent progress of the FEM technology enabled straightforward modeling of the SRM. However, the optimization of the phase current waveform by the FEM technology is based on the trial and error approach in search for the desirable phase current waveform from a huge number of possible phase current waveforms. Hence, the whole calculation may be needed every time the SRM design is changed. For avoiding this problem, this paper rather constructs the analytical formulation of the proposed phase current waveform, which can cover the arbitrary inductance profile including the commercially available SRMs.

The remainder of this paper comprises 5 sections. First, section II briefly reviews the previous phase current waveform [35][36]. Section III presents the analytical derivation method of the proposed phase current waveform. Then, section IV presents an example of the proposed phase current waveform for a commercially available SRM. This section also presents the performance comparison between the proposed and previous phase current waveforms based on a simple analytical SRM model. Effectiveness of the proposed waveform was tested by the experiment in section V. Finally, section VI gives the conclusions.

II. Previous Phase Current Waveform

This section reviews the derivation of the previously proposed phase current waveform based on the three-phase concentrated-winding SRM as presented in Fig. 1. For convenience, we neglect the magnetic coupling between the phase windings. The following discussion is focused on phase U. However, a similar discussion also stands for the other phases because of the symmetry between the phases.

First, we formulate the magnetic co-energy contributed by phase U, denoted as E'_U, as a function of the phase current i_U and the electric angle θ_E. (The origin of θ_E is taken at the rotor pole aligned position.) As widely known E'_U is proportional to i_U^2 if the magnetic saturation is not considered. Hence, we approximate E'_U to have the following form:

$$E'_U = K_2(\theta_E) i_U^2, \tag{1}$$

where $K_2(\theta_E)$ is the given coefficients of the SRM under consideration as a function of θ_E; κ_{21}, κ_{22}, … are the Fourier's expansion coefficients of $K_2(\theta_E)$. As is in many SRM designs, we simply assume that $K_2(\theta_E)$ is an even function of θ_E.

By utilizing (1), we can formulate the torque contributed by phase U, denoted as τ_U, and the input current contributed by phase U, denoted as i_{EU}, as

$$\tau_U = P \frac{\partial K_2}{\partial \theta_E} i_U^2, \tag{2}$$

$$\begin{aligned} i_{EU} &= \frac{\Omega}{V_{dc}} \left(\frac{dE_U}{d\theta_E} + \tau_U \right) = \frac{\Omega}{V_{dc}} \left\{ \frac{d}{d\theta_E} \left(i_U \frac{\partial E'_U}{\partial i_U} - E'_U \right) + \tau_U \right\} \\ &= \frac{\Omega}{V_{dc}} \left\{ \frac{d}{d\theta_E} \left(K_2 i_U^2 \right) + \tau_U \right\}, \end{aligned} \tag{3}$$

where Ω is the angular velocity and V_{dc} is the voltage of the DC power supply to the inverter that drives the SRM, and E_U is the magnetic energy contributed by phase U. (We neglect the high-frequency ripple in the input current caused by the switching.)

Because of the symmetry between the phases, the torque contributed by phases V and W, as well as the input current contributed by phases V and W, must have the same waveform as τ_U and i_{EU} with the phase shift of $-2/3\pi$ and $-4/3\pi$, respectively. Hence, both of τ_U and i_{EU} must not contain the harmonics of multiples of three in order to have no ripples in the total torque and the total input current.

For the practical derivation of the phase current, we introduce the two functions $g(\theta_E)$ and $p(\theta_E)$ defined as

$$g(\theta_E) = K_2(\theta_E) i_U^2(\theta_E), \quad p(\theta_E) = \frac{\partial \ln K_2(\theta_E)}{\partial \theta_E}. \tag{4}$$

Then, we approximate these functions to have the form:

$$\begin{aligned} g(\theta_E) = A_0 &+ A_1 \sin\theta_E + A_2 \sin 2\theta_E + \cdots + A_5 \sin 5\theta_E \\ &+ B_1 \cos\theta_E + B_2 \cos 2\theta_E + \cdots + B_5 \cos 5\theta_E. \end{aligned} \tag{5}$$

$$p(\theta_E) = \kappa_1 \sin\theta_E + \kappa_2 \sin 2\theta_E + \cdots + \kappa_5 \sin 5\theta_E. \tag{6}$$

Substituting (4)–(6) into (2) and (3) and seeking for the solution that both of τ_U and i_{EU} do not contain the harmonics of multiples of three, we obtain the following necessary conditions:

$$A_4 = -\frac{\kappa_4 - \kappa_2 + (\kappa_1 - \kappa_5)\dfrac{\kappa_5}{\kappa_4}}{(K_1 - K_5)\left(\dfrac{\kappa_2}{\kappa_4} - \dfrac{\kappa_1\kappa_5}{\kappa_4^2}\right) + \kappa_1 - \dfrac{\kappa_2\kappa_5}{\kappa_4}} A_1, \quad (7)$$

$$B_4 = \frac{2\kappa_3 A_0 + \left\{\kappa_2 + \kappa_4 - (\kappa_1 + \kappa_5)\dfrac{\kappa_5}{\kappa_4}\right\}}{(\kappa_1 + \kappa_5)\left(\dfrac{\kappa_2}{\kappa_4} - \dfrac{\kappa_1\kappa_5}{\kappa_4^2}\right) + \kappa_1 - \dfrac{\kappa_2\kappa_5}{\kappa_4}} B_1, \quad (8)$$

$$A_2 = -\frac{\kappa_5}{\kappa_4} A_1 - \left(\frac{\kappa_2}{\kappa_4} - \frac{\kappa_1\kappa_5}{\kappa_4^2}\right) A_4, \quad (9)$$

$$B_2 = -\frac{\kappa_5}{\kappa_4} B_1 - \left(\frac{\kappa_2}{\kappa_4} - \frac{\kappa_1\kappa_5}{\kappa_4^2}\right) B_4, \quad (10)$$

$$A_5 = -\frac{\kappa_5}{\kappa_4} A_4, \quad B_5 = -\frac{\kappa_5}{\kappa_4} B_4. \quad (11)$$

Among parameters A_0-A_5 and B_0-B_5, A_0, A_1, and B_1 can be chosen freely as far as $g(\theta_E)$ remains positive at any θ_E, whereas the others are determined according to (7)–(11). Therefore, the previous method can generate various phase current waveforms that can achieve the simultaneous elimination of the input current ripple and the torque ripple. Once the parameters A_0, A_1, and B_1 are chosen, the phase current waveform can be calculated according to

$$i_U(\theta_E) = \sqrt{g(\theta_E)/K_2(\theta_E)}. \quad (12)$$

Because (7)–(11) are linear relations among A_0-A_5 and B_0-B_5, arbitrary attenuation or magnification of a solution of $g(\theta_E)$ is also the solution. Therefore, once a waveform of $i_U(\theta_E)$ is derived according to (12), this waveform can be attenuated or magnified to adjust the average output torque without generating the input current ripple or the torque ripple.

III. Proposed Phase Current Waveform

A. Overview of Derivation Process

Next, this section presents the derivation method of the proposed phase current waveform, which further considers the magnetic saturation. Similarly, as in the previous section, we consider the three-phase concentrated winding SRM and we neglect the magnetic coupling among the phases. However, the magnetic co-energy is assumed to have the following form to model the nonlinear flux-current property, caused by the magnetic saturation.

$$E'_U = K_2(\theta_E) i_U^2 + K_3(\theta_E) i_U^3 + \cdots + K_{m+1}(\theta_E) i_U^{m+1}, \quad (13)$$

where $K_2(\theta_E)$, $K_3(\theta_E)$, …, $K_{m+1}(\theta_E)$ are the given functions of θ_E determined by the motor structure. Then, τ_U and i_{EU}, i.e. the torque and the input current contributed by phase U, should be modified as

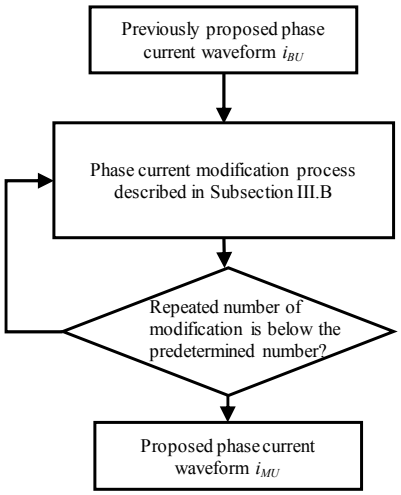

Fig. 2. Flow chart of derivation process of proposed phase current wveform.

$$\tau_U = P\left(\frac{\partial K_2}{\partial \theta_E} i_U^2 + \frac{\partial K_3}{\partial \theta_E} i_U^3 + \cdots + \frac{\partial K_{m+1}}{\partial \theta_E} i_U^{m+1}\right), \quad (14)$$

$$i_{EU} = \frac{\Omega}{V_{dc}}\left\{\frac{d}{d\theta_E}\left(K_2 i_U^2 + 2K_3 i_U^3 + \cdots + mK_{m+1} i_U^{m+1}\right) + \tau_U\right\}, \quad (15)$$

Our purpose is to find a waveform for i_U that can eliminate the harmonics of multiples of three from (14) and (15) at a desired average output torque. However, the direct calculation of this solution is generally complicated. Therefore, this paper adopted a step-by-step optimization approach.

Figure 2 depicts the flow-chart of the derivation process of the proposed phase current waveform. In this process, we start from the previously proposed phase current waveform at the predetermined average output torque. Then, based on the waveform, we search for a slightly modified phase current waveform that can further reduce the harmonics of multiples of three from τ_U and i_{EU} but does not affect the output torque. By repeating this process, we finally obtain the phase current waveform that can sufficiently eliminate the harmonics of multiples of three from τ_U and i_{EU}. The following subsection describes the analytical calculation method that derives the slightly modified phase current waveform based on the original phase current waveform.

B. Derivation of Modified Phase Current Waveform

Let i_{BU} and i_{MU} be the original phase current waveform and the slightly modified phase current waveform, respectively. Then, the relation between i_{BU} and i_{MU} can be expressed as

$$i_{MU}(\theta_E) = i_{BU}(\theta_E) + \Delta i_U(\theta_E), \quad (16)$$

where $\Delta i_U(\theta_E)$ is a small deviation of i_{MU} from i_{BU}. In this discussion, we assume that Δi_U has a far smaller amplitude than i_{MU} and i_{BU}.

Substituting (16) into (14) and (15), and ignoring the terms of order higher than the second in Δi_U, we obtain

$$\tau_U = Pq(\theta_E) + Pf(\theta_E)\Delta i_U, \tag{17}$$

$$i_{EU} = \frac{\Omega}{V_{dc}}\left[\frac{d}{d\theta_E}\{e(\theta_E) + h(\theta_E)\Delta i_U\} + \tau_U\right], \tag{18}$$

where $q(\theta_E)$, $f(\theta_E)$, $e(\theta_E)$, and $h(\theta_E)$ are given functions of θ_E defined as (we regard i_{BU} as a given waveform)

$$q(\theta_E) = \frac{\partial K_2}{\partial \theta_E} i_{BU}^2 + \frac{\partial K_3}{\partial \theta_E} i_{BU}^3 + \cdots + \frac{\partial K_{m+1}}{\partial \theta_E} i_{BU}^{m+1}, \tag{19}$$

$$f(\theta_E) = 2\frac{\partial K_2}{\partial \theta_E} i_{BU} + 3\frac{\partial K_3}{\partial \theta_E} i_{BU}^2 + \cdots + (m+1)\frac{\partial K_{m+1}}{\partial \theta_E} i_{BU}^m, \tag{20}$$

$$e(\theta_E) = K_2 i_{BU}^2 + 2K_3 i_{BU}^3 + \cdots + mK_{m+1} i_{BU}^{m+1}, \tag{21}$$

$$\begin{aligned} h(\theta_E) &= 2K_2 i_{BU} + 6K_3 i_{BU}^2 + 12K_4 i_{BU}^3 \\ &\quad + \cdots + m(m+1)K_{m+1} i_{BU}^m. \end{aligned} \tag{22}$$

Let $s(\theta_E)$ and $l(\theta_E)$ be functions of θ_E defined as

$$s(\theta_E) = q(\theta_E) + f(\theta_E)\Delta i_U, \tag{23}$$

$$l(\theta_E) = e(\theta_E) + h(\theta_E)\Delta i_U. \tag{24}$$

Then, the sufficient condition for simultaneous elimination of the total input current ripple and the total torque ripple is that $s(\theta_E)$ and $l(\theta_E)$ do not have the harmonics of multiples of three. Therefore, we should determine the waveform of Δi_U that eliminates the harmonics of multiples of three from $s(\theta_E)$ and $l(\theta_E)$. Eliminating Δi_U from (23) and (24) yields

$$s(\theta_E) = g(\theta_E)l(\theta_E) + k(\theta_E), \tag{25}$$

where $g(\theta_E)$ and $k(\theta_E)$ are functions of θ_E defined as

$$g(\theta_E) = \frac{f(\theta_E)}{h(\theta_E)}, \quad k(\theta_E) = q(\theta_E) - \frac{f(\theta_E)e(\theta_E)}{h(\theta_E)}. \tag{26}$$

Note that $g(\theta_E)$ and $k(\theta_E)$ can be readily calculated from the magnetic co-energy model presented in (13) and the original phase current waveform i_{BU}. Hence, we should search for a pair of $s(\theta_E)$ and $l(\theta_E)$ that do not contain the harmonics of multiples of three under the given functions of $g(\theta_E)$ and $k(\theta_E)$. Once a pair of $s(\theta_E)$ and $l(\theta_E)$ is found, a desired waveform of Δi_U can be readily calculated as

$$\Delta i_U = \frac{l(\theta_E) - e(\theta_E)}{h(\theta_E)}. \tag{27}$$

For simplifying the calculation in search for a pair of $s(\theta_E)$ and $l(\theta_E)$, we neglect the harmonics of θ_E higher than 6 contained in $g(\theta_E)$ and $k(\theta_E)$. Hence, $g(\theta_E)$ and $k(\theta_E)$ are approximated as

$$\begin{aligned} g(\theta_E) &= C_0 + C_1\cos\theta_E + C_2\cos 2\theta_E + C_3\cos 3\theta_E \\ &\quad + C_4\cos 4\theta_E + C_5\cos 5\theta_E + C_6\cos 6\theta_E \\ &\quad + D_1\sin\theta_E + D_2\sin 2\theta_E + D_3\sin 3\theta_E \\ &\quad + D_4\sin 4\theta_E + D_5\sin 5\theta_E + D_6\sin 6\theta_E, \end{aligned} \tag{28}$$

$$\begin{aligned} k(\theta_E) &= T_0 + T_1\cos\theta_E + T_2\cos 2\theta_E + T_3\cos 3\theta_E \\ &\quad + T_4\cos 4\theta_E + T_5\cos 5\theta_E + T_6\cos 6\theta_E \\ &\quad + U_1\sin\theta_E + U_2\sin 2\theta_E + U_3\sin 3\theta_E \\ &\quad + U_4\sin 4\theta_E + U_5\sin 5\theta_E + U_6\sin 6\theta_E. \end{aligned} \tag{29}$$

Furthermore, we simply assume that $l(\theta_E)$ has the following form, remembering that $l(\theta_E)$ should not contain the harmonics of multiples of three:

$$\begin{aligned} l(\theta_E) &= X_0 + X_1\cos\theta_E + X_2\cos 2\theta_E + X_4\cos 4\theta_E \\ &\quad + X_5\cos 5\theta_E + Y_1\sin\theta_E + Y_2\sin 2\theta_E \\ &\quad + Y_4\sin 4\theta_E + Y_5\sin 5\theta_E. \end{aligned} \tag{30}$$

Substituting (28)–(30) into (25), we can derive the requirement conditions among coefficients X_0–X_5 and Y_1–Y_5 for eliminating the harmonics of multiples of three from the resultant $s(\theta_E)$. Consequently, the requirement conditions for the coefficients are obtained as

$$\begin{aligned} X_4 = -\{&2D_2U_6 + 2D_1U_3 + 2C_2T_6 - 2C_1T_3 + 2X_0D_2D_6 \\ &+ (X_1D_2 + X_2D_1 - Y_1C_2 - Y_2C_1)D_5 \\ &+ (X_2D_2 + X_1D_1 - Y_2C_2 - Y_1C_1)D_4 + 2X_0D_1D_3 \\ &+ (X_1D_1 + Y_1C_5 + Y_2C_4 + Y_1C_1)D_2 + X_2D_1^2 \\ &+ (-Y_2C_5 + Y_1C_4 + Y_1C_2 + 2Y_2C_1)D_1 + 2X_0C_2C_6 \\ &+ (X_1C_2 - X_2C_1)C_5 + (X_2C_2 - X_1C_1)C_4 - 2X_0C_1C_3 \\ &- X_1C_1C_2 - X_2C_1^2\}/(D_2^2 - D_1^2 + C_2^2 - C_1^2). \end{aligned} \tag{31}$$

$$\begin{aligned} X_5 = \{&2D_1U_6 + 2D_2U_3 + 2C_1T_6 - 2C_2T_3 + 2X_0D_1D_6 \\ &+ (X_2D_2 + X_1D_1 - Y_2C_2 - Y_1C_1)D_5 \\ &+ (X_1D_2 + X_2D_1 - Y_1C_2 - Y_2C_1)D_4 + 2X_0D_2D_3 \\ &+ (X_2D_1 - Y_2C_5 - Y_1C_4 + 2Y_1C_2 + Y_2C_1)D_2 + X_1D_2^2 \\ &+ (Y_1C_5 + Y_2C_4 + Y_2C_2)D_1 + 2X_0C_1C_6 \\ &+ (X_1C_1 - X_2C_2)C_5 + (X_2C_1 - X_1C_2)C_4 - 2X_0C_2C_3 \\ &- X_2C_1C_2 - X_1C_2^2\}/(D_2^2 - D_1^2 + C_2^2 - C_1^2). \end{aligned} \tag{32}$$

$$\begin{aligned} Y_4 = -\{&2C_2U_6 - 2C_1U_3 - 2D_2T_6 - 2D_1T_3 + 2X_0C_2D_6 \\ &+ (Y_1D_2 - Y_2D_1 + X_1C_2 - X_2C_1)D_5 \\ &+ (Y_2D_2 - Y_1D_1 + X_2C_2 - X_1C_1)D_4 - 2X_0C_1D_3 \\ &+ (Y_1D_1 - 2X_0C_6 - X_1C_5 - X_2C_4 - X_1C_1)D_2 + Y_2D_1^2 \\ &+ (-X_2C_5 - X_1C_4 - 2X_0C_3 - X_1C_2 - 2X_2C_2)D_1 \\ &+ (Y_1C_2 + Y_2C_1)C_5 + (Y_2C_2 + Y_1C_1)C_4 - Y_1C_1C_2 \\ &- Y_2C_1^2\}/(D_2^2 - D_1^2 + C_2^2 - C_1^2), \end{aligned} \tag{33}$$

TABLE I. SPECIFICATIONS OF EXPERIMENTAL SWITCHED RELUCTANCE MOTOR

Model number	RB165SR-96CSRM (Motion System Tech. Inc.)
Rate value	1.2kW, 96V, 6000rpm
Structure	Stator: 12 poles, Rotor: 8 poles, Number of turns: 14T/pole

TABLE II. COEFFICIENTS *Kij* USED FOR MAGNETIC CO-ENERGY MODEL OF EXPERIMENTAL SWITCHED RELUCTANCE MOTOR

	i=1	*i*=2	*i*=3	*i*=4	*i*=5	*i*=6
K_{i0}	3.5×10^{-4}	2.9×10^{-6}	-1.6×10^{-7}	2.1×10^{-9}	-1.3×10^{-11}	3.0×10^{-14}
K_{i1}	3.3×10^{-4}	3.6×10^{-6}	-2.1×10^{-7}	2.9×10^{-9}	-1.8×10^{-11}	4.3×10^{-14}
K_{i2}	8.2×10^{-5}	-6.5×10^{-7}	-2.3×10^{-8}	4.9×10^{-10}	-3.7×10^{-12}	9.8×10^{-15}
K_{i3}	2.5×10^{-5}	-1.6×10^{-6}	3.0×10^{-8}	-2.4×10^{-10}	8.5×10^{-13}	-8.5×10^{-16}
K_{i4}	2.9×10^{-5}	-7.0×10^{-7}	4.0×10^{-9}	5.7×10^{-11}	-8.0×10^{-13}	2.7×10^{-15}
K_{i5}	1.5×10^{-5}	-5.4×10^{-7}	5.5×10^{-9}	2.0×10^{-12}	-3.2×10^{-13}	1.3×10^{-15}
K_{i6}	7.8×10^{-6}	-5.7×10^{-7}	1.4×10^{-8}	-1.6×10^{-10}	8.8×10^{-13}	-1.9×10^{-15}

$$\begin{aligned} Y_5 = \{&2C_1U_6 - 2C_2U_3 - 2D_1T_6 - 2D_2T_3 + 2X_0C_1D_6 \\ &+ (-Y_2D_2 + Y_1D_1 - X_2C_2 + X_1C_1)D_5 + Y_1D_2^2 \\ &+ (-Y_1D_2 + Y_2D_1 - X_1C_2 + X_2C_1)D_4 - 2X_0C_2D_3 \\ &+ (-X_2C_5 - X_1C_4 - 2X_0C_3 - X_1C_2 - 2X_2C_2)D_1 \\ &+ (Y_2D_1 - X_2C_5 - X_1C_4 - 2X_0C_3 - 2X_1C_2 - X_2C_1)D_2 \\ &+ (-2X_0C_6 - X_1C_5 - X_2C_4 - X_2C_2)D_1 \\ &+ (Y_2C_2 + Y_1C_1)C_5 + (Y_1C_2 + Y_2C_1)C_4 - Y_2C_1C_2 \\ &- Y_1C_2^2\}/(D_2^2 - D_1^2 + C_2^2 - C_1^2). \end{aligned} \quad (34)$$

Using these requirement conditions, we can determine a pair of $s(\theta_E)$ and $l(\theta_E)$. Similarly, as in the previous section, there is a variety of possible pairs of $s(\theta_E)$ and $l(\theta_E)$. However, we should choose a pair that does not affect the output torque of the previous waveform i_{BU}.

Once $s(\theta_E)$ and $l(\theta_E)$ are chosen, Δi_U can be determined according to (27). Consequently, the modified phase current waveform is determined as $i_{MU}=i_{BU}+\Delta i_U$. It is noteworthy that this derivation method of the modified phase current waveform contains much approximation. Therefore, the resultant modified phase current waveform cannot completely eliminate the input current ripple and the torque ripple. This is the reason why we repeated the process of deriving the modified phase current waveform to achieve sufficient elimination of the input current ripple and the torque ripple.

IV. EXAMPLE OF PROPOSED PHASE CURRENT WAVEFORM

This section presents an example of the proposed phase current waveform calculated for a commercially available SRM. This SRM was also utilized in the experiment, described in section V. Table I shows the specifications of this SRM.

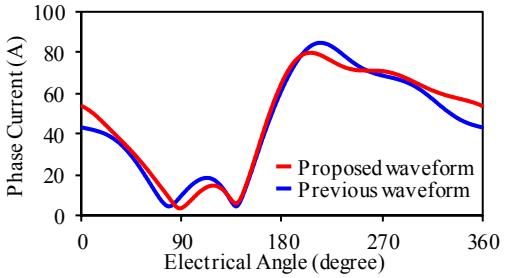

Fig. 3. Proposed and previous phase current waveforms calculated for the experimental motor.

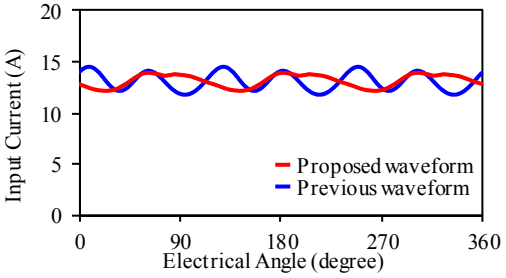

(a) Input current ripple

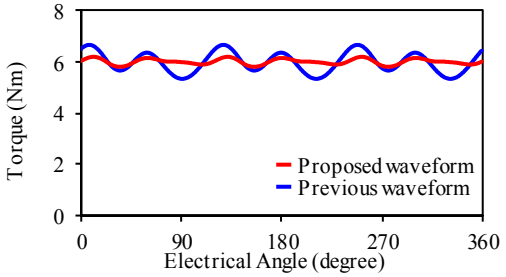

(b) Torque ripple

Fig. 4. Input current ripple and torque ripple of proposed and previous phase current waveforms calculated based on analytical model of experimental motor.

The magnetic co-energy model of the SRM was constructed based on the experimentally measured relation between the phase magnetic flux and the phase current. In this model, the functions $K_2(\theta_E)$, $K_3(\theta_E)$, … were expressed by the following form [37]:

$$\begin{aligned} K_i(\theta_E) = K_{i0} &+ K_{i1}\cos\theta_E + K_{i2}\cos2\theta_E + K_{i3}\cos3\theta_E \\ &+ K_{i4}\cos4\theta_E + K_{i5}\cos5\theta_E + K_{i6}\cos6\theta_E, \end{aligned} \quad (35)$$

where i and j are the natural numbers from 2 to 5 and from 0 to 6, respectively; and K_{ij} are the Fourier expansion coefficients of $K_i(\theta_E)$. Consequently, the parameters for the magnetic co-energy model is determined as shown in Table II.

Based on the magnetic co-energy model, we derived the proposed phase current waveform for the average output torque of 6.0Nm, in which the magnetic saturation affects both the torque and the input current. We started from the previously proposed phase current waveform for the output torque of 6.0Nm and repeated twice the modification process of the phase current waveform to finally obtain the proposed phase current waveform.

Figure 3 shows the proposed and previous phase current waveforms. The overall shape of the proposed phase current

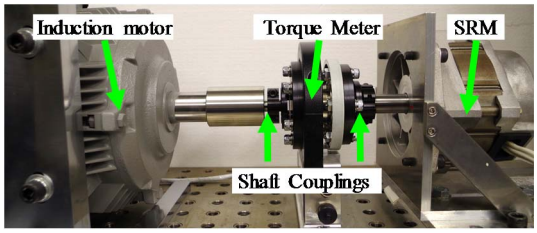

Fig. 5. Photograph of motor test bench

TABLE III. SPECIFICATIONS OF MOTOR TEST BENCH

Instrument	Specifications
Torque meter	T40B 50Nm (HBM Corp.)
Shaft Coupling	SFF-060SS-T059N (Miki Pulley co., LTD.) SFF-060SS-T060N (Miki Pulley co., LTD.)
Induction motor	TFO-K 3.7kW 2P 200V (Hitachi Industrial Equipment Systems Co., LTD.)

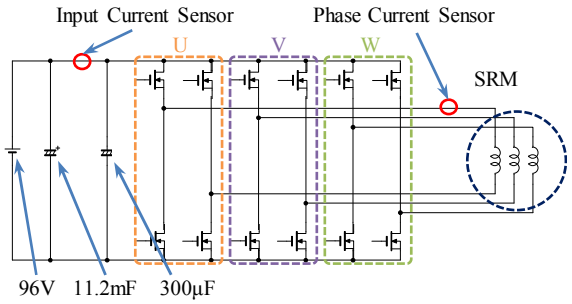

Fig. 6. Schematic diagram of inverter for driving experimental switched reluctance motor.

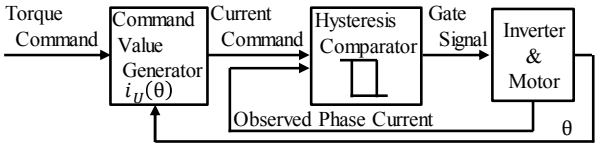

Fig. 7. Control diagram of inverter.

waveform was similar to the previous phase current waveform. However, the proposed waveform has a slightly smaller peak current. The effective values of the proposed and previous waveforms were 53.0A_{rms} and 52.3A_{rms}, respectively. Consequently, the proposed waveform does not result in the increase in the copper loss.

Next, the input current and the output torque were analytically calculated and compared between the proposed and previous phase current waveforms. The input current and output torque contributed by one phase was calculated according to (14) and (15) using the analytical SRM model presented in Table II. The DC power supply voltage V_{dc} and the angular velocity Ω was set at 96V and 209.4rad/s (2000rpm), respectively. Based on the result, the total input current and the total output torque were calculated as the sum of all the three phases.

Figure 4 shows the comparison result of the total input current waveform and the total output torque waveform between the proposed and previous phase current waveforms The results indicate that the proposed phase current waveform successfully reduced both of the input current ripple and the torque ripple. In fact, the peak-to-peak value of the ripple was reduced from 2.6$A_{p\text{-}p}$ to 1.7$A_{p\text{-}p}$ in the input current ripple and from 1.3$Nm_{p\text{-}p}$ to 0.4$Nm_{p\text{-}p}$ in the torque ripple. Furthermore, the root-mean-square value of the ripple was reduced from 0.8A_{rms} to 0.6A_{rms} in the input current ripple and from 0.4Nm_{rms} to 0.1Nm_{rms} in the torque ripple.

V. EXPERIMENT

An experiment was carried out to verify the effectiveness of the proposed phase current waveform. In this experiment, the input current ripple and the torque ripple were evaluated and compared between the proposed and previous phase current waveforms. We utilized the SRM, considered in the previous section, to test the phase current waveforms shown in Fig. 3.

Figure 5 shows a motor test bench used in this experiment. We utilized the induction motor for the mechanical load. Therefore, in the test bench, the SRM and the induction motor were connected mechanically via an instantaneous torque meter and couplings. The specification of the SRM is the same as Table I. The other specifications regarding this test bench are listed in Table III.

The SRM was driven using an inverter. The schematic diagram of the inverter is shown in Fig. 6. The inverter comprised three full-bridge circuits each made of four power MOSFETs, which is a common inverter topology for driving the SRM. This inverter was controlled to supply the predetermined phase current waveforms. Figure 7 depicts the control diagram of the inverter. In this experiment, we adopted the hysteresis current tracking control. The hysteresis width was set at 6.0A.

In this experiment, the torque ripple was measured at 250rpm, whereas the input current ripple was measured at 2000rpm. The torque ripple was measured at a low rotation speed because of the limited bandwidth of the instantaneous torque meter. Additionally, this rotation speed is beneficial for avoiding the parasitic mechanical resonance of the motor test bench. On the other hand, the input current ripple was measured at a comparatively high rotational speed. The reason is that power conversion efficiency tends to be low at a low rotational speed. The equation of the input curent ripple (15) is based on the approximation that the motor can convert the electric power into the kinetic power without any power loss. Therefore, operation at extremely low efficiency was avoided because low efficiency may deteriorate the reduction of the input current ripple.

Figure 8 and 9 show the evaluation results. As can be seen in the figure, both of the input current ripple and the torque ripple were successfully reduced in the proposed phase current waveform. In fact, the peak-to-peak value of the ripple was reduced from 22.4$A_{p\text{-}p}$ to 16.1$A_{p\text{-}p}$ in the input current ripple and from 2.3$Nm_{p\text{-}p}$ to 1.4$Nm_{p\text{-}p}$ in the torque ripple. Furthermore, the root-mean-square value of the ripple was reduced from 4.8A_{rms} to 3.4A_{rms} in the input current ripple and from 0.6Nm_{rms} to 0.4Nm_{rms} in the torque ripple.

Consequently, the experiment successfully supported the effective reduction of the input current ripple and the torque ripple by the proposed phase current waveform.

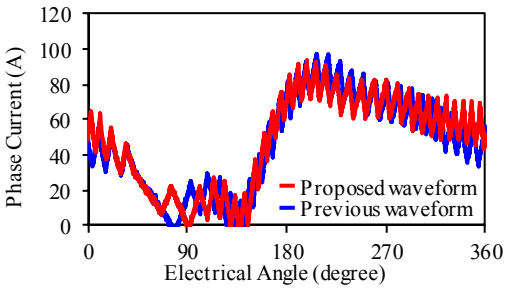

(a) Phase current

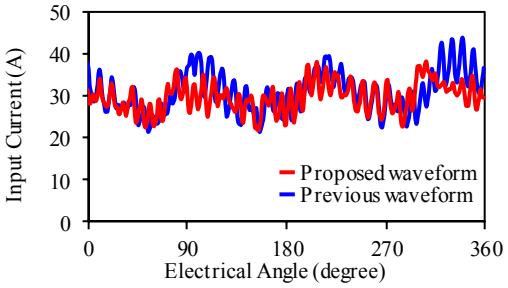

(b) Input current ripple

Fig. 8. Experimental evaluation results of input current ripple of proposed and previous phase current waveforms at 2000rpm.

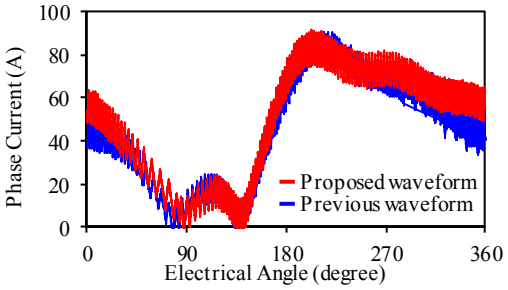

(a) Phase current waveforms

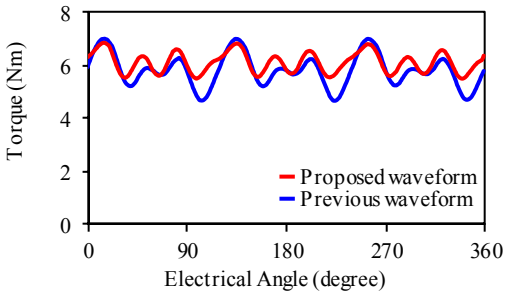

(b) Torque ripple

Fig. 9. Experimental evaluation results of torque ripple of proposed and previous phase current waveforms at 250rpm.

VI. Conclusions

The application of SRMs to the vehicular propulsion is hindered by comparatively large input current ripple and torque ripple. Although the previous study has proposed a phase current waveform to eliminate these ripples, this previous study derived the waveform by neglecting the magnetic saturation for a straightforward calculation of the waveform. Consequently, the elimination of these ripples was greatly deteriorated at high torque output, in which the magnetic saturation significantly affects the input current and the torque.

For solving this issue, this paper proposed an improved phase current waveform. The proposed waveform is based on the nonlinear magnetic model considering the magnetic saturation. Therefore, the proposed waveform can cover the operating condition of high output torque, in which the magnetic saturation cannot be neglected. The proposed waveform can be analytically driven using the non-linear magnetic co-energy model. This indicates that the proposed phase current waveform can be straightforwardly calculated for arbitrary SRMs without the trial and error, as far as the analytical model is given. The experiment verified the effective reduction in the input current ripple and the torque ripple, supporting the effectiveness of the proposed phase current waveform.

References

[1] Z. Q. Zhu and C. C. Chan, “Electrical machine topologies and technologies for electric, hybrid, and fuel cell vehicles,” in Proc. IEEE Vehicle Power Propulsion Conf., Harbin, China, pp. 1–6, Sept. 2008.

[2] W. Suppharangsan and J. Wang, “Experimental validation of a new switching technique for DC-link capacitor minimization in switched reluctance machine drives,” in Proc. IEEE Int. Electric Machines Drives Conf., Chicago, USA, pp. 1031–1036, May 2013.

[3] I. Husain and M. Ehsani, “Torque ripple minimization in switched reluctance motor drives by PWM current control”, IEEE Trans. Power Electron., Vol. 11, No. 1, pp. 83-88, Jan. 1996.

[4] A. M. Stankovic, G. Tadmor, Z. J. Coric, and I. Agirman, “On torque ripple reduction in current-fed switched reluctance motors”, IEEE Trans. Ind. Electron., Vol. 46, No. 1, pp. 177-183, Feb. 1999.

[5] L. Venkatesha and V. Ramanarayanan, “A comparative study of pre-computed current methods for torque ripple minimization in switched reluctance motor”, in Proc. IEEE Ind. Appl. Conf., Rome, Italy, Vol. 1, pp. 119-125, Oct. 2000.

[6] I. Agirman, A. M. Stankovic, G. Tadmor, and H. Lev-Ari, “Adaptive torque-ripple minimization in switched reluctance motors”, IEEE Trans. Ind. Electron., Vol. 48, No. 3, pp. 664-672, Jun. 2001.

[7] P. L. Chapman and S. D. Sudhoff, “Design and precise realization of optimized current waveforms for an 8/6 switched reluctance motor drive”, IEEE Trans. Power Electron., Vol. 27, No. 1, pp. 76-83, Jan. 2002.

[8] L. O. de Araujo, P. Henriques, P. J. Costa Branco, L. G. B. Rolim, and W. I. Suemitsu, “Proposition of an offline learning current modulation for torque-ripple reduction in switched reluctance motors: design and experimental evaluation”, IEEE Trans. Ind. Electron., Vol. 49, No. 3, pp. 665-676, Jun. 2002.

[9] A. D. Cheok and Y. Fukuda, “A new torque and flux control method for switched reluctance motor drive”, IEEE Trans. Power Electron., Vol. 17, No. 4, pp. 543-557, Jul. 2002.

[10] Y. Zheng, H. Sun, Y. Dong, and W. Wang, “Torque ripple minimization with current oriented method for switched reluctance motor”, in Proc. IEEE Intl. Conf. Elect. Mach. Syst., South Korea, pp. 1640-1644, Oct. 2007.

[11] N. Chayopitak, R. Pupadubsin, K. Tungpimolrut, P. Somsiri, P. Jitkreeyan, and S. Kachapornkul, “A adaptive low-ripple torque control of switched reluctance motor for small electric vehicle”, in Proc. Intl. Conf. Elect. Mach. Syst. (ICEMS2008), Wuhan, China, pp. 3327-3332, Oct. 2008.

[12] D.-H. Lee, J. Liang, Z.-G. Lee, and J.-W. Ahn, “A simple nonlinear logical torque sharing function for low-torque ripple SR drive”, IEEE Trans. Ind. Electron., Vol. 56, No. 8, pp. 3021-3028, Aug. 2009.

[13] X. D. Xue, K. W. E. Cheng, and S. L. Ho, “Optimization and evaluation of torque-sharing functions for torque ripple minimization in switched reluctance motor drives”, IEEE Trans. Power Electron., Vol. 24, No. 9, pp.2076-2090, Sept. 2009.

[14] B. Blanque and A. Doria-Cerezo, “Torque ripple minimization for a switched reluctance motor”, in Proc. European Conf. Power Electron. Appl. (EPE2009), Barcelona, Spain, pp. 1-8, Sept. 2009.

[15] C. Pavlitov, H. Chen, Y. Gorbounov, T. Tashev, T. Georgiev, and W. Xing, “Switched reluctance motor torque ripples reduction by the aid of adaptive reference model”, in Proc. Intl. Sym. Power Electron.

Elect. Drives Automation Motion (SPEEDAM2010), Pisa, Italy, pp. 1276-1279, Jun. 2010.

[16] V. P. Vujicic, "Minimization of torque ripple and copper losses in switched reluctance drive", IEEE Trans. Power Electron., Vol. 27, No. 1, pp. 388-399, Jan. 2011.

[17] M. M. Namazi, S. M. Saghaian-Nejad, A. Rashidi, and H. A. Zarchi, "Passivity-based adaptive sliding mode speed control of switched reluctance motor drive considering torque ripple reduction", in Proc. IEEE Intl. Elect. Mach. Drives Conf. (IEMDC2011), Niagara Falls, ON, USA, pp. 1480-1485, May 2011.

[18] J. Fort, B. Skala, and V. Kus, "The torque ripple reduction at the drive with the switched reluctance motor", in Proc. IEEE Intl. Power Electron. Motion Ctrl. Conf. (EPE-PEMC2012), Novi Sad, Servia, DS2a.16-1-4, Sept. 2012.

[19] R. Mitra and Y. Sozer, "Torque ripple minimization of switched reluctance motors through speed signal processing", in Proc. IEEE Energy Conversion Congr. Expo., Pittsburgh, PA,USA, pp. 1366-1373, Sept. 2014.

[20] W. Yi, Q. Ma, and J. Hu, "Torque ripple minimization of switched reluctance motors by controlling the phase currents during commutation", in Proc. Intl. Conf. Elect. Mach. Syst. (ICEMS2014), Hangzhou, China, pp. 1866-1870, Oct. 2014.

[21] J. Ye, B. Bilgin, and A. Emadi, "An extended-speed low-ripple torque control of switched reluctance motor drives", IEEE Trans. Power Electron., Vol. 30, No. 3, pp. 1457-1470, Mar. 2015.

[22] H. Makino, S. Nagata, T. Kosaka, and N. Matsui, "Instantaneous current profiling control for minimizing torque ripple in switched reluctance servo motor", in Proc. IEEE Energy Conversion Congr. Expo., Montreal, QC, Canada, pp. 3941-3948, Sept. 2015.

[23] N. K. Sheth and K. R. Rajagopal, "Optimum Pole Arcs for a Switched Reluctance Motor for Higher Torque With Reduced Ripple", IEEE Trans. Magnetics, Vol. 39, No. 5, pp. 3214-3216, Sept. 2003.

[24] J. W. Lee, H. S. Kim, B. I. Kwon, and B. T. Kim, "New Rotor Shape Design for Minimum Torque Ripple of SRM Using FEM" IEEE Trans. Magnetics, vol. 40, no. 2, pp. 754-757, Mar. 2004.

[25] Y. K. Choi, H. S. Yoon, and C. S. Koh, "Pole-Shape Optimization of a Switched-Reluctance Motor for Torque Ripple Reduction," IEEE Trans. Magnetics, vol. 43, no. 4, pp. 1797-1800, Apr. 2007.

[26] S.-M. Jang, D.-J. You, Y.-H. Han, and J.-P. Lee, "Analytical design and dynamic characteristics of switched reluctance motor with minimum torque ripple", in Proc. Intl. Conf. Elect. Mach. Syst. (ICEMS2007), Seoul, South Korea, pp. 1236-1239, Oct. 2007.

[27] T. Higuchi, K. Suenaga, and T. Abe, "Torque ripple reduction of novel segment type switched reluctance motor by increasing phase number", in Proc. Intl. Conf. Elect. Mach. Syst. (ICEMS2009), Tokyo, Japan, pp. 1-4, Nov. 2009.

[28] A. Siadatan, M Asgar, V. Najmi, and E. Afjei, "A novel method for torque ripple reduction in 6/4 two rotor stack switched reluctance motor", in Proc. European Conf. Power Electron. Appl. (EPE2011), Birmingham, UK, pp. 1-10, Aug. 2011.

[29] M. A. Tavakkoli and M. Moallem, "Torque ripple mitigation of double stator switched reluctance motor (DSSRM) using a novel rotor shape optimization", in Proc. IEEE Energy Conversion Congr. Expo., Raleigh, NC, USA, pp. 848-852, Sept. 2012.

[30] Y. Li and D. C. Aliprantis, "Optimum stator tooth shapes for torque ripple reduction in switched reluctance motors", in Proc. IEEE Elect. Mach. Drives Conf., Chicago, IL, USA, pp. 1037-1044, May 2013.

[31] F. Yi and W. Cai, "Repetitive control-based current ripple reduction method with a multi-port power converter for SRM drive," in Proc. IEEE Transportation Electrification Conf. Expo., Dearborn, MI, USA, pp. 1-6, Jun. 2015.

[32] W. Cai and F. Yi, "An Integrated Multiport Power Converter With Small Capacitance Requirement for Switched Reluctance Motor Drive," IEEE Trans. Power Elect., vol. 31, no. 4, pp. 3016-3026, Apr. 2016.

[33] L. Du, B. Gu, J. S. Lai, and E. Swint, "Control of pseudo-sinusoidal switched reluctance motor with zero torque ripple and reduced input current ripple," in Proc. IEEE Energy Conversion Congr. Expo., Denver, CO, USA, pp. 3770-3775, Sept. 2013.

[34] E. Swint and J. Lai, "Switched reluctance motor without torque ripple or electrolytic capacitors," in Proc. IEEE Energy Conversion Congr. Expo., Phoenix, AZ, USA, pp. 1657-1663, Sept. 2011.

[35] T. Kusumi, T. Hara, K. Umetani, and E. Hiraki, "Simple control technique to eliminate source current ripple and torque ripple of switched reluctance motors for electric vehicle propulsion," in Proc. IECON 2016 - 42nd Annual Conf. of the IEEE Industrial Elect. Society, Florence, Italy, pp. 1876-1881, Oct. 2016.

[36] T. Kusumi, T. Hara, K. Umetani, and E. Hiraki, "Simple analytical derivation of magnetic flux profile eliminating source current ripple and torque ripple of switched reluctance motors for electric vehicle propulsion," in Proc. 2017 IEEE Applied Power Elect. Conference and Exposition (APEC), Tampa, FL, USA, pp. 3142-3149, Mar. 2017.

[37] T. Hara, T. Kusumi, K. Umetani, and E. Hiraki, "A simple behavior model for switched reluctance motors based on magnetic energy," in Proc. Intl. Power Electron. Motion Control Conf. (IPEMC2016), Hefei, China, May. 2016.